

Survivability: A Unifying Concept for the Transient Resilience of Deterministic Dynamical Systems

Frank Hellmann^{*},^{1,*} Paul Schultz^{*},^{1,2,†} Carsten Grabow,^{1,‡} Jobst Heitzig,¹ and Jürgen Kurths^{1,2,3,4}

¹*Potsdam Institute for Climate Impact Research, P.O. Box 60 12 03, 14412 Potsdam, Germany*

²*Department of Physics, Humboldt University of Berlin, Newtonstr. 15, 12489 Berlin, Germany*

³*Institute for Complex Systems and Mathematical Biology,*

University of Aberdeen, Aberdeen AB24 3UE, United Kingdom

⁴*Department of Control Theory, Nizhny Novgorod State University,
Gagarin Avenue 23, 606950 Nizhny Novgorod, Russia*

(Dated: August 30, 2022)

The notion of a part of phase space containing desired (or allowed) states of a dynamical system is important in a wide range of complex systems research. It has been called the safe operating space, the viability kernel or the sunny region. In this paper we define the notion of survivability: Given a random initial condition, what is the likelihood that the transient behaviour of a deterministic system leaves the region of desirable states. In three conceptual examples we show that this basic measure captures notions of fundamental interest for climate models, transient chaos, and synchronisation. This covers applications to linear and non-linear, multistable and monostable systems. We also derive a semi-analytic lower bound for the survivability of linear systems with polygonal safe operating space.

We then apply the concept in the case of the second order Kuramoto model, interpreted as a model of the power grid, where the type of resilience measured by survivability is of great practical interest. We show that our lower bound is a good predictor for the survivability of the power grid in realistic operating regimes.

Our numerical and semi-analytic work shows that the type of resilience measured by survivability is not captured by common measures of stability such as relaxation time, basin stability, the master stability function and other asymptotic concepts.

Keywords: TODO

I. INTRODUCTION

In almost all dynamical systems applicable to the real world, the stability of the system's stationary states is of key interest. Perturbations are never truly absent, and initial data is never exactly determined. Nevertheless, the asymptotic stability of the system's attractors ensures that we can still extract sensible long-term information from our dynamical models.

Complementary to the notion of stability, one can analyze whether the system will reach a desirable state. This becomes important when a model represents a system that we have influence on, either because we engineer its fundamental behavior, or because there are management options. We often want to design the dynamics, or our interventions, such as to more easily keep the system in such a desired state. Note that desirable states are typically not stationary states.

For the traditional notion of asymptotic stability against infinitesimal perturbations, the key mathematical concept is the analysis of the linearized dynamics, for instance by means of the Lyapunov exponent or master stability function [24, 29].

Multistable systems [12, 30, 34] have more than one stable attractor [21], and thus potentially exhibit a wide range of different asymptotic behaviours. The key question then becomes from which initial state which attractor is reached, that is, the basin of attraction of an attractor. Most work so far focused on the geometry of the basin of attraction of desirable attractors, for example by finding Lyapunov functions [6, 8, 42].

An idea that has recently been found to be useful is to study a more elementary property, not which states go to an attractor, but just how many. This quantity, the volume of the basin of attraction of a given attractor (possibly within some finite volume subset of phase space) can then be interpreted as the resilience of the system in the face of a random, non-small perturbation (within the finite volume subset studied). It quantifies the probability that the strongly non-linear response to such a perturbation will lead the system to a different, undesirable attractor. This probability is called the basin stability of an attractor [20]. Basin stability quantifies the stability of an attractor taking large deviations into account. This is important for a number of applications where relevant system deviations are typically not small, for example in power grids.

One of the key appealing features of basin stability is that, by studying just the volume rather than the shape of the basin of attraction, it becomes numerically tractable to analyze even very high-dimensional systems. It was also shown that the information revealed by the

* hellmann@pik-potsdam.de

† pschultz@pik-potsdam.de

‡ grabow@pik-potsdam.de

* These authors contributed equally to the research presented.

volume of the basin genuinely complements the information provided by the Lyapunov exponents of the linearized system [20].

There are, however, two major drawbacks when estimating basin stability. On the one hand, the measure relies on correctly identifying the asymptotic behavior of a system, which might in some cases be difficult to detect, typically requires prior knowledge about the attractor's nature, and is only meaningful in multistable systems. On the other hand, a basin stability estimation is insensitive to undesired transient behavior of the system, i.e. if the trajectory visits an undesired part of the phase space where the system would take damage that is not modeled intrinsically. This renders basin stability a too rough measure for some applications.

In this paper we introduce a new stability and resilience measure, the *survivability* $S(t)$ of a dynamical system. This is the fraction of initial conditions giving rise to trajectories that stay within a desirable region for a given time t . The set of these initial conditions will be called *basin of survival*.

As opposed to basin stability or a linear(-ized) analysis, the *survivability* is concerned not just with the asymptotic behavior of the system, but depends strongly on the transient dynamics. As opposed to basin stability it is applicable in unstable, monostable, or multistable, linear or non-linear systems. For example, in the case of transient chaos [35, 36, 40], we have long, interesting transients but potentially just a single global attractor. Treating a small region around the global attractor as undesirable, the survivability captures the typical lifetime of the interesting transients in the vicinity of chaotic repellers, a fundamental quantity of high interest.

The application of the survivability concept is especially appropriate when interventions happen at the same timescale as the system dynamics, or when entering an undesirable region is deadly. Further, survivability thereby retains and improves the desirable numerical properties of basin stability. The entire curve $S(t)$ can be evaluated at a computational complexity not exceeding that of a basin stability estimation, potentially revealing much more information. Hence, a survivability analysis is applicable to very high-dimensional systems as well.

For linear systems with polygonal desirable region, we derive a closed form lower bound on the *infinite-time survivability* as well as a semi-analytic, stronger bound that becomes exact in the case of a purely imaginary spectrum, precisely when the linearized system no longer reveals anything about asymptotic stability. These bounds reveal that the survivability of linear systems depends strongly on the eigenvectors of the linear dynamics, rather than just the eigenvalues.

To demonstrate the utility of survivability as a system property, we apply it to three paradigmatic model systems:

i) The first is a simple two-dimensional model of carbon stock dynamics [2]. This system exhibits both the property that the undesirable states are deadly and that

in some parameter regimes there is only a single stable attractor of the asymptotic dynamics.

ii) The second example is a simple system of integrate-and-fire neurons [11, 22, 39]. These exhibit very interesting long-term irregular transients, but asymptotically have a global periodic attractor where the neurons are in a state of phase-synchronization. Considering the synchronized state as undesirable, the integrate-and-fire neurons are an example of a system in which neither asymptotic nor basin stability are applicable. The survivability reveals the length of the transients. It can be interpreted to measure the resilience of the chaotic regime, in the sense that it reveals the risk to become synchronized given a particular interval between external stimuli.

iii) The third example is an effective network model of the power grid [13, 25]. This was one of the first systems for which basin stability was thoroughly studied [19]. However, as basin stability is insensitive to transient behavior, it unrealistically classifies trajectories that have massive transient frequency deviations, at which the power grid would long have collapsed, as stable. Secondly, upon detection of a disturbance, active management would set in at the same time scale as the system dynamics. Hence, the power grid is an example where the undesirable region is deadly and management options operate at the system dynamics time scale. We study a conceptual two-dimensional, two-node model of the power grid, and then apply the concept of survivability to study a full 472-dimensional model of the Scandinavian transmission grid. We indeed find that basin stability and infinite-time survivability of the system are not correlated with each other in this example. Further we find that for realistic maximum frequency deviations, the lower bound on the survivability of the linearized system is an excellent predictor for the total survivability.

All our examples have in common that there are externalities in the system which are not or cannot be modeled. Such as the influence of dramatic climate changes on society, control mechanisms in the power grid or external stimuli for a network of neurones. A survivability analysis is a way to deal with the occurrence of such external influences iff they can be transformed into the definition of a desirable subset of the phase space.

II. SURVIVABILITY, DEFINITIONS AND BASIC PROPERTIES.

Imagine the time evolution of a particle in a complicated potential landscape where attractors are given by local minima, or, alternatively, a penguin, wishing to ski down a mountain going the fastest route possible in Fig. 1. The system is multi-stable as the penguin might end up in the goal or the valley. Starting location A and starting location B both are in the basin of attraction of the goal. However, starting in location A leads the penguin to a cliff. Crossing the cliff the fastest route possible

will almost certainly lead to the penguin sliding the rest of the way to the goal on its back; not a desirable state. However, not one that is intrinsically modelled by the (potential) landscape. Whether a cliff is undesirable or not, might well depend on a further externality, like the skill level of our penguin.

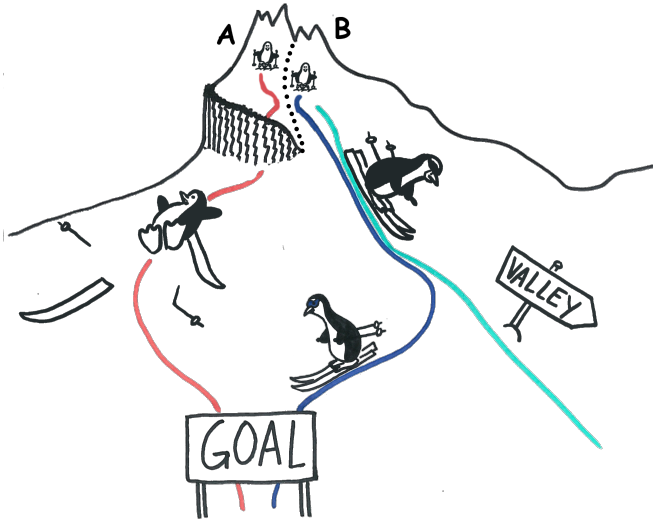


Figure 1. **Survivability cartoon:** (Color online.) A penguin can ski down the mountain starting anywhere on the slope. Starting at A the penguin will tumble over the cliffs, reaching an undesirable state. Starting at B the penguin will reach the goal standing on its feet. Starting even further to the right, it might end up in the valley, which might or might not be desirable.

If reaching the valley and being on the back are considered undesirable states, the basin of survival are those starting positions beneath the cliff and those on the right hand side of the dotted line, but left of the divide to the valley. In this case the basin of attraction of the goal contains the basin of survival. If reaching the valley is not objectionable to our penguin, the basin of survival crosses the boundary of the basin of attraction.

More formally, consider a dynamical system with states x in a state space X giving rise to trajectories $x(t)$ under some evolution map $\sigma(t)$. Now we define a desirable region $X^+ \subset X$ with its complement $X^- = X \setminus X^+$, where the former contains all states x that are stated to be desirable. In the penguin example X^- would contain the cliff and the valley. In the context of Earth System science, such a desirable region has variously been called the *safe operating space* within *planetary boundaries* [31] or the *sunny region* [14].

We define the survivability $S(t)$ of the dynamical system at time t to be the fraction of trajectories starting in X^+ that stay within X^+ for the entire duration $[0, t]$. Put another way, if entering the region X^- terminates the system, $S(t)$ is the fraction of trajectories starting in X^+ still alive after time t . We call the part of X^+ from which trajectories start that stay alive at least for time t

the *finite-time* or *t-time basin of survival* X_t^S . We then have

$$S(t) = \frac{\text{Vol}(X_t^S)}{\text{Vol}(X^+)}, \quad (1)$$

where Vol is an inner measure on X determining the volume of the sets X_t^S and X^+ in the phase space. By construction, $S(t)$ takes values on the unit interval.

We define the total survivability $S = S_\infty$ as the limit

$$S_\infty = \lim_{t \rightarrow \infty} S(t). \quad (2)$$

Each t -time basin of survival is a subset of the previous ones $X_t^S \supset X_{t'}^S$ (for $t' > t$), as trajectories returning to X^+ after leaving it once do not contribute to $X_{t'}^S$. Hence, $S(t)$ is monotonically decreasing and bounded by 0 from below, therefore the limit in Eqn. 2 exists. The use of an inner measure here avoids subtleties involving non measurable sets, like fractal [27, 28] or riddled [1, 17] basins of attraction.

Note however that if X^+ is an open set, and the map $\sigma(t) : X \rightarrow X$ is continuous for all t , then the images of X^+ under $\sigma(t)^{-1}$ are also open. As $X_t^S = \bigcup_{0 < t' < t} \sigma(t')^{-1} X^+$ is a union of open sets it is itself open and therefore measurable if Vol is a Borel measure. Thus in this important special case, which covers all applications we are considering in this paper, no such subtleties exist.

In some applications the choice for the set X^+ might have an infinite volume, even though X_t^S becomes finite for sufficiently large t . In that case one can still consider the unnormalised volume $\text{Vol}(X_t^S)$ as a relative measure of the survivability of a system.

A. Conditional survivability

The conditional survivability $S^C(t)$ measures the response of the system to restricted perturbations. For example, we might be interested in the survivability, given perturbations that are localized at a node in a network. Given a subset of the state space $C \subset X$, we define the conditional survivability as the fraction of trajectories starting in $X^+ \cap C$ that stay in X^+ . That is

$$S^C(t) = \frac{\text{Vol}|_C(X_t^S \cap C)}{\text{Vol}|_C(X^+ \cap C)}, \quad (3)$$

where $\text{Vol}|_C$ is an inner measure on the smallest submanifold containing C . In the case of a network and perturbations at a single node, the phase space typically is the product of phase spaces at the nodes, and the volume measure likewise factorizes, thus there are natural choices for C and $\text{Vol}|_C$.

B. Numerically estimating survivability

One advantage shared by survivability and basin stability [20] is that they can be efficiently estimated by randomly sampling starting conditions. A trajectory either survives/converges or not, therefore we can regard the sampling as a Bernoulli process with probability given by $S(t)$ or the basin stability S_B , hence the standard error of the mean SEM of a trial with N draws is simply

$$SEM = \sqrt{\frac{S(t)(1-S(t))}{N}}. \quad (4)$$

As a crucial consequence, the standard error of a survivability estimation does not depend on the dimensionality of the system. Further, the condition that a trajectory has left X^+ tends to be easier to evaluate in practise than whether the trajectory is asymptotically approaching a fixed point. Furthermore, in numerical simulations, an integration might be stopped once X^+ has been left.

C. Relationship to basin stability

Let us further consider the relationship between basin stability and survivability. Consider the union of all attractors A in X . Following the terminology of [14], we split the set A into desirable attractors A^+ and undesirable attractors A^- . Define X_A^+ and X_A^- to be the basin of attraction of A^+ and A^- respectively. The basin stability of A^+ with respect to some initial region X^0 is then defined as

$$S_B = \frac{\text{Vol}(X^0 \cap X_A^+)}{\text{Vol}(X^0)}. \quad (5)$$

Note that defining basin stability requires knowledge of the respective attractor. Efficiently evaluating it numerically requires a criterion to evaluate whether the system will converge to a certain attractor.

Let us assume that the sunny region cleanly separates the set of attractors, that is, there are some attractors that are entirely sunny and others that are entirely shaded, but none that intersect both regions. In this case, we can establish a quantitative relationship between basin stability and survivability. We can choose $A^+ = A \cap X^+$ (i.e. desirable attractors are contained inside the sunny region), and we know that asymptotically the trajectories converge either to A^- or A^+ or diverge. Thus every trajectory that does not contribute to the basin stability also has to leave the sunny region eventually and can not contribute to the survivability either. Thus if

$$\begin{array}{ll} & A^+ = A \cap X^+ \\ \text{and} & X^0 = X^+, \\ \text{then} & S_B \geq S_\infty. \end{array} \quad (6)$$

The difference between the two values is exactly the measure of initial conditions whose trajectories leave the sunny region intermittently but eventually return to it and stay. Thus we see that whether basin stability or survivability is the appropriate measure depends on whether the forbidden region is merely unpleasant, and we want our stay there to be finite, or whether the forbidden region is deadly and we absolutely do not want the system to enter it at all.

D. Relationship to similar concepts

Survivability has been studied in the context of stochastic systems, i.e. the concept of the so-called first hitting time and survival probability [3, 10]. The first hitting time t measures when a system is expected to first hit the forbidden region X^- . The cumulative of the probability of first hitting the undesirable region before t is then $1 - S(t)$. Our definitions given above can be seen as deterministic generalizations of these concepts. The role of stochasticity in the evolution is replaced by taking the average over all (or some) initial conditions.

In the context of control theory, a similar concept to the basin of survival is the viability kernel defined by Aubin et. al. in the context of viability theory [4, 5]. They introduce the notion of an environment K that contains all desirable states. Within the environment, there is the so-called viability kernel V [7, 18] as the set of all initial conditions from which the system *can* stay within the environment. This basically is a more general version of our infinite-time basin of survival for non-deterministic systems or systems with multiple evolution paths and a management process. Consequently, $K \setminus V$ corresponds to the set of finite-time surviving states in deterministic systems. The viability kernel's volume is proposed as a measure of the degree of viability [5], in the limit of no control it thus reduces to our total survivability. However, we are not aware of numerical applications for deterministic systems in the context of viability theory.

Just as in the case of basin stability, we find that it is advantageous to restrict our attention to the volume rather than the geometry of the set of surviving states. The numerical and analytic simplifications open up the application of these concepts to many interesting systems.

III. ANALYTIC RESULTS FOR LINEAR SYSTEMS

An important special case, which is tractable analytically, is the total survivability S for the case of a linear dynamic in $X = \mathbb{R}^N$, the Lebesgue measure $\text{Vol}(X) = \int_X dx^N$, and a polyhedral sunny region given by m linear conditions $y_k \cdot x(t) < 1$ for a set of vectors y_k , $k = 1 \dots m$ in \mathbb{R}^N . In this case we can give a lower bound on $\text{Vol}(X_\infty^S)$ that is easy to evaluate.

In this section we briefly give the results we actually make use of in the applications in Sec. IV C and V. There we demonstrate that the semi-analytic bound captures the survivability of the system quite accurately in practical examples. In appendix B we show detailed derivations, as well as further analytic results.

Consider a linear system of ordinary differential equations

$$\dot{x}(t) = Lx(t) \quad (7)$$

with $x \in X = \mathbb{R}^N$ and $L \in \mathbb{R}^{N \times N}$ with all eigenvalues having non-positive real parts. In general, L has a complex spectrum. The eigenvectors v_j of the complex eigenvalues are real or come in complex conjugate pairs, from which we pick one eigenvector each. We then define the $N \times N$ matrix \mathbb{V} by stacking the eigenvectors, or their real and imaginary parts respectively, against each other as column vectors:

$$\mathbb{V} = [v_1, \dots, \text{Re}(v_{j'}), \dots, -\text{Im}(v_{j'}), \dots]. \quad (8)$$

This allows us to translate initial conditions into the eigenvector basis by setting $c' = \mathbb{V}^{-1}x(0)$, and combining $c'_{j'}$ into complex numbers as appropriate $c_{j'} = c'_{j'} + ic'_{j''}$. Then the trajectory describes an exponential decay along the real eigenvectors and an inward spiral in the $\text{Re}(v_{j'})$, $\text{Im}(v_{j'})$ plane that is parametrized by $c_{j'}$. We can then obtain an upper bound for the inner product of the trajectory starting at $x(0)$ with a boundary vector y_k by maximizing the contribution of each motion separately.

Now, setting $y_{kj} := y_k \cdot v_j$ for v_j real, and $y_{kj} := |y_k \cdot v_j|$ for v_j complex, this leads to the estimate:

$$\begin{aligned} \max_{t \in [0; \infty[} |y_k \cdot x(t)| &\leq \sum_{j=1}^{n_0} y_{kj} c_j \\ &+ \sum_{j=n_0+1}^{n_r} \max(0, y_{kj} c_j) \\ &+ \sum_{j=n_r+1}^n y_{kj} |c_j| \end{aligned} \quad (9)$$

where the first sum is over real eigenvectors corresponding to null eigenvalues, the second is over nonzero real eigenvectors and the last is over the complex eigenvectors.

Setting the right hand side of Eqn. 9 smaller than 1 defines a region V_c in \mathbb{R}^N spanned by the real and imaginary parts of the coefficients c_j . It then follows that:

$$\text{Vol}(X_\infty^S) \geq \sqrt{\det \mathbb{V} \mathbb{V}^T} \text{Vol}(V_c). \quad (10)$$

The inequalities Eqn. 9 together with the matrix \mathbb{V} can be used to efficiently estimate the total survivability as well as the conditional survivability. Remarkably, for

systems with purely imaginary spectrum, the bounds of Eqn. 9 and Eqn. 10 hold with equality.

In appendix B we also derive a lower bound for $\text{Vol}(V_c)$.

This lower bound demonstrates that for the survivability of a linear system, the eigenvectors play a crucial role. In fact, the eigenvalues do not enter the bound at all, except in terms of classifying the corresponding eigenvectors in separate classes. This demonstrates that the survivability captures substantially different information about the linear system than eigenvalue based stability and resilience measures like relaxation time, or the master stability function.

IV. THREE PARADIGMATIC MODEL SYSTEMS

A. A carbon cycle model from climate science

In order to demonstrate the potential of the survivability concept, we apply it to a two-dimensional carbon cycle model from climate science which has been recently introduced [2]. This is a conceptual model with the aim to reproduce the non-linear dynamics of the carbon cycle in the Earth system. The boundaries of the *survival region* are closely related to the concept of planetary boundaries [31].

The model equations for the atmospheric (c_a), marine (c_m) and terrestrial (c_t) carbon stocks are given by

$$\begin{aligned} \dot{c}_m &= \alpha_m (c_a - \beta c_m) \\ \dot{c}_t &= NEP(c_a, c_t) - \alpha c_t \\ c_a &= 1 - c_m - c_t \end{aligned} \quad (11)$$

where α_m denotes the atmosphere-ocean diffusion coefficient, β the carbon-solubility in sea water factor, α the human terrestrial carbon offtake rate and $NEP(c_a, c_t)$ the net ecosystem production, a complex non-linear relationship between the atmospheric and terrestrial carbon stocks (see [2] for further details). Note that the total amount of carbon is kept constant, leaving us with the marine (c_m) and terrestrial (c_t) carbon stocks as independent variables.

Part of the phase space of the model are states with virtually no terrestrial carbon, so-called *desert states*. While the model can recover from such states and eventually reach high terrestrial carbon states again, entering such a state would lead to the collapse of human civilization and thus, tragically, our model would no longer be valid after entering this regime. Hence, we define the set of desirable states X^+ as the complement of the desert states plus a safety margin m :

$$X^+ = \{(c_a, c_m, c_t) \in X : c_t > m\}. \quad (12)$$

The finite-time basin of survival is given by

$$X_t^S = \{(c_a, c_m, c_t) \in X : \bigvee_{0 < t' \leq t} c_t(t') > m\}. \quad (13)$$

The safety margin should at no time, during the transient or asymptotic behavior, be crossed.

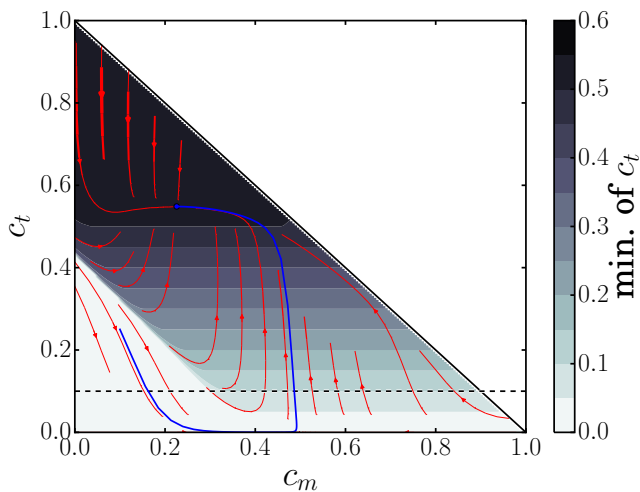


Figure 2. **Phase space analysis with $\alpha = 0.1$.** (Color online.) For each initial condition, the color indicates the minimum terrestrial carbon stock over the whole time evolution. An example trajectory with a long excursion to the desert state ($c_t < m$) is plotted in blue, the stream plot indicates the vector field of the right-hand-side (cf. Eqn. 11). The dashed black line indicates the value of the safety margin $m = 0.1$.

A phase plane analysis for this model is illustrated in Fig. 2. Of special importance here are those trajectories (exemplified by the blue trajectory in Fig. 2) that first cross the safety margin, i.e. are not desirable due to the very low terrestrial carbon stocks c_t , but eventually will return to the safe operating space X^+ . These trajectories are counted for the basin stability estimation, since they eventually approach the attractor, but are disregarded for the survivability, since they cross the safety margin during the transient period.

Note that in this case we estimate a finite-time survivability for the entire simulated time evolution of the system. Given that the asymptotic behavior sets in earlier than the simulation ends, this is a good estimate for the infinite-time survivability.

By varying the human carbon offtake α in Eqn. 11, the system undergoes a bifurcation changing the number of attractors (around $\alpha = 0.35$) as illustrated in Fig. 3. While this bifurcation, which is known to be a saddle-node bifurcation [2], has a drastic impact on the basin stability estimation, the survivability only changes marginally in this interval. On the other hand, the behaviour in the interval $\alpha \in [0; 0.35]$ shows how the basin stability estimation becomes insensitive to system changes if the multistability is lost, i.e. if there is only a single attractor (in this case with non-zero c_t). The crucial question whether trajectories stay in a safe regime is thus not captured by the basin stability measure, but can be answered with the survivability concept.

In [20] it was argued that basin stability can also serve

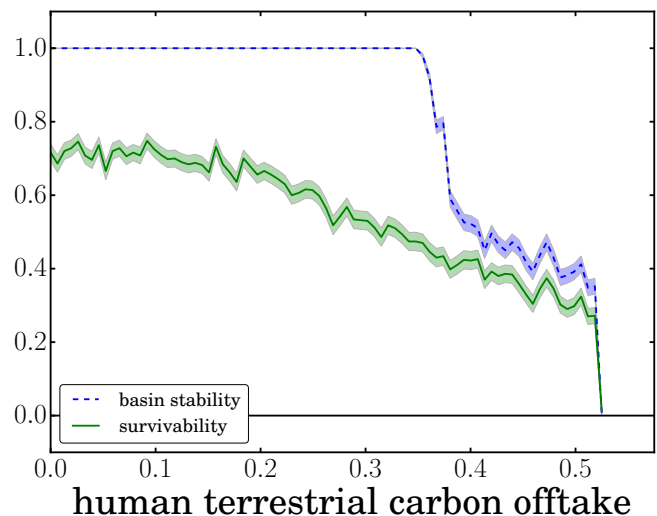


Figure 3. **Variation of human carbon offtake:** (Color online.) Basin stability and survivability estimates for different values of the terrestrial human carbon offtake α . For the survivability estimation we assumed a safety margin $m = 0.1$

as a better early warning indicator of a tipping point than other measures. Here we see that a survivability estimation mirrors the trend in the system's behavior, i.e. how the set of surviving states depends on system parameters, while the basin stability remains fixed at its plateau value. Hence, survivability can serve as a complementary, and in some scenarios better early warning sign than basin stability.

B. Network of integrate-and-fire Oscillators

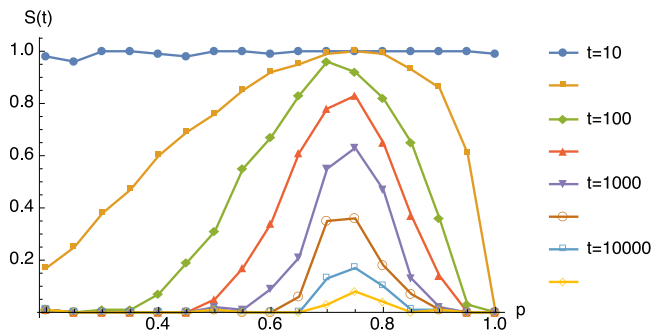


Figure 4. **Survivability for pulse-coupled neuronal networks:** (Color online.) Finite-time survivability $S(t)$ for given survival times t vs. the network parameter p . For each value of p we average over an ensemble of 100 network realizations, each with randomly drawn initial conditions.

As another motivational example we consider a network of N pulse-coupled oscillators [11, 15, 22]. In the network every oscillator $j = 1 \dots N$ is connected to another oscillator $i \neq j$ by a directed link with probability

p . A phase variable $\phi_j(t) \in [0, 1]$ specifies the state of each oscillator j at time t . The oscillators interact on a directed graph by sending and receiving pulses. After a delay time τ this pulse induces a phase jump in the receiving oscillator i which depends on its instantaneous phase $\phi_i(t + \tau)$, the excitatory coupling strength $\varepsilon_{ij} \geq 0$, and on whether the input is sub- or supra-threshold (cf. appendix A).

We now study the convergence from arbitrary initial conditions to periodic orbit attractors, in which several synchronized groups of oscillators (clusters) coexist [41].

The finite-time survivabilities for a directed network of $N = 16$ pulse-coupled oscillators in dependence on the average connectivity p are illustrated in Fig. 4. For each value of p we create an ensemble of 100 network realizations. The randomly chosen initial phase vectors for each realization are distributed uniformly in $[0, 1]^N$.

Here it is not meaningful to apply the concept of basin stability, since all different network realizations with their associated initial conditions eventually lead to a fully synchronous state. However, our concept of survivability reveals the highly non-linear, non-monotonic dependence on the network connectivity p . While the survivability of transient dynamic states is small for networks with low and high connectivity values p , it becomes very large for intermediate connectivities, even for only weakly diluted networks (Fig. 4). The finite-time survivability reveals a new, collective time scale that is much larger than the natural period, 1, of an individual oscillator and the delay time, τ , of the interactions.

These long, irregular transients are the main property of interest for the system, motivating their study in [41]. The dependence of the average lifetime of the transient chaotic trajectories on p was already studied *ibidem*. Survivability basically reveals the same information, but in the sense of an intrinsic resilience against synchronization. If the system is subject to repeated stimuli/perturbations with time interval Δt , the probability to survive without the oscillators synchronizing in between these stimuli is exactly $S(\Delta t)$. Survivability again is a natural and informative measure of resilience in this system, however, this time not against perturbations, but against getting trapped in an unwanted boring corner of phase space.

C. The two-node power grid

Power grids are subject to a variety of failures and perturbations and there are numerous studies concerning asymptotic stability analysis, e.g. [9, 23], and recent approaches to a non-linear stability assessment [19, 33]. However, contrary to common model assumptions, the dynamical system does usually not evolve freely after a perturbation. If the system does not return to a stable operating state after a typical time span of a few seconds or if predefined thresholds are exceeded, control mechanisms that would require independent modelling

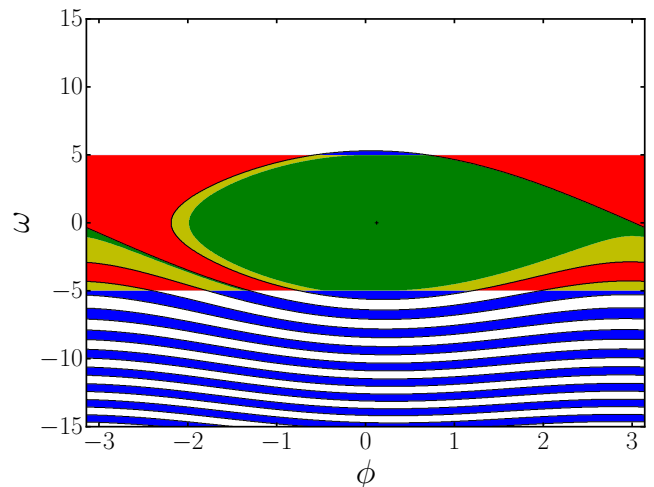


Figure 5. **Phase space classification:** (Color online.) The central green area is the infinite-time basin of survival, while the yellow and red areas contain finite-time surviving states. The union of the blue, yellow and green regions is the fixed point's basin of attraction, while trajectories starting in the white or red regions approach the limit cycle solution. The frequency threshold is set to $\omega_{crit.} = \pm 5$.

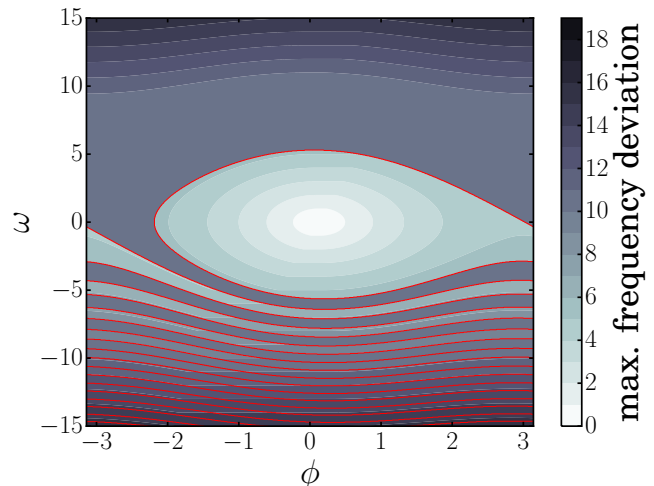


Figure 6. **Simulated maximum frequency deviations:** (Color online.) Field of maximum frequency deviations measured over the time evolution of the two-node power grid (Eqn. (14)) for each initial condition. For comparison with Fig. 5, we give the basin of attraction's boundaries in red.

are triggered.

The long-term behavior and stability of the system is thus a question for control theory rather than just dynamics. Conversely, the transient dynamics, and the question whether there is a temporary amplification of perturbations, is critical to whether the control has to be activated in the first place, or the system is intrinsically resilient to such perturbations.

Before we are going to apply the survivability concept

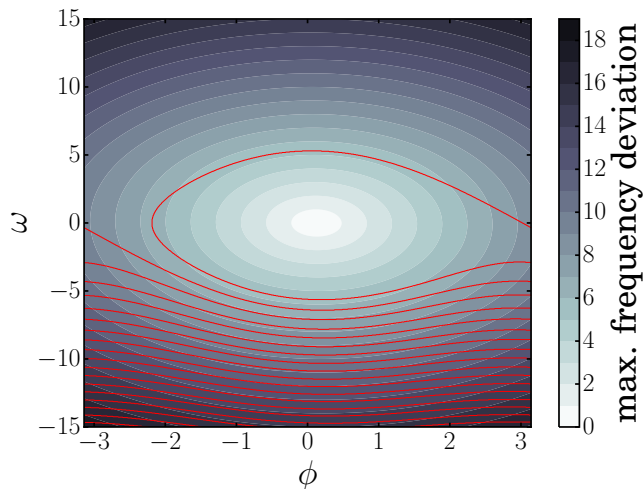


Figure 7. **Approximated maximum frequency deviations:** (Color online.) Analytic upper bound for the maximum frequency deviation (Eqn. (9)) of the linearized system. For comparison with Fig. 5, we give the basin of attraction's boundaries in red.

to a large power grid network, we pick the smallest possible system, consisting of only one pair of a generator and a motor, as an illustrative example. The basic dynamics is given by the two-dimensional system

$$\begin{aligned}\dot{\phi} &= \omega \\ \dot{\omega} &= 2P - \alpha\omega - 2K \sin \phi\end{aligned}\quad (14)$$

where ϕ and ω are the phase and phase velocity differences between the generator and the motor. Given that $P < K$ and $\alpha \leq \pi P/(4\sqrt{K})$ the system is bistable with the coexistence of a stable focus (node) and a limit cycle [16]. Here we choose $P = 1$, $K = 6$ and $\alpha = 0.1$. The fixed point corresponds to the stationary operating state, whereas the limit cycle solution (frequency oscillations) is a state that needs to be prevented in order to avoid the tripping of generators. Frequency deviations are usually kept very small in real power grids, with typical thresholds of ± 0.2 Hz [37]. Here, we work with ± 0.15 Hz which is safely below that critical threshold and corresponds to a phase velocity deviation of $|\omega| \approx 5$ in our units.

The basin of attraction of this system is illustrated in Fig. 5. Concerning survivability, there is a subdivision in three different sets. The sunny region contains infinite- (central green region) and finite-time surviving states (yellow and red regions in the band). Trajectories commencing from the remaining states within the basin of attraction (blue region) eventually reach the attractor asymptotically. Note that there are also finite-time surviving states outside the basin of attraction (red region).

In contrast, Fig. 6 shows the maximum frequency deviation of a trajectory starting at a particular point. Measuring this bound for a sample of initial conditions can be used to determine the infinite-time basin of survival.

For comparison, Fig. 7 shows the analytic bound (Eqn. 9) applied to the linearization of Eqn. 14.

There is good agreement between the upper bound and the measured maximum frequency deviations within the basin of attraction, close to the fixed point. The linearized dynamics is, of course, not multistable. Hence the bound must fail at the basin boundaries, where multistability becomes the defining feature. Further it can not take into account the periodicity of the phase space, we have to limit the linearized phase space to $\pm\pi$ around the fix point by hand.

If we consider the allowed region to be defined by the maximum frequency deviation, the level lines of Fig. 6 and Fig. 7 denote the simulated and approximated basin of survival. We can observe a few initial features here:

- As pointed out above in Sec. II, the basin of attraction contains the infinite-time basin of survival, if the undesired attractor lies entirely outside of the allowed region X^+ defined by the frequency bounds.
- For realistic small deviations, the upper bound applied to the linear approximation provides an excellent picture of the infinite time basin of survivability. The fact that the behaviour at large phase perturbations is not captured accurately is irrelevant to measuring S in this case.
- Finite-time and infinite-time surviving states can easily be distinguished in the above case numerically, as the former are short-lived in comparison to the simulation time. This feature might not survive in systems in which very different time scales are important.

V. APPLICATION: GENERAL POWER GRIDS

We can now turn to the motivating application of the concept of survivability, realistic power grids as modelled by a system of coupled swing masses. We will study the *single node basin of survival*, that is, the conditional basin of survival on the product of a fixed point of the dynamics and the phase space of a single node of the power grid in the sense of Eqn. 3. We will describe the space that the survivability is conditioned on further down.

The network of coupled swing masses approach is the current standard baseline model for the frequency dynamics of power grids. It is known as the *swing equation* or the second order Kuramoto model, and is used for short-term frequency stability studies in power grids. The various ways in which a power grid can be modelled using the swing equation are discussed in [25]. Limits to its applicability are discussed, for example, in [38].

All our simulations are performed with at least 300 samples, leading to a SEM of less than 0.03 for $S(t) = 0.5$ in the worst case (cf. Sec. II B). We evaluate the survivability up to $t = 100$, at which point a steady state

has typically been established, and the asymptotic value of the survivability is reached.

While basin stability captures the overall ability of the system to avoid permanent frequency oscillations, it does not directly capture the resilience of the system against large perturbations. Instead, as discussed above for the two node system, it is the ability of the system to keep perturbations under fixed frequency thresholds which is crucial. As for the two-node system in the previous section, we will study this form of resilience using both numerical simulations and the analytic approximations we have derived. The former will allow us to compare the survivability of the system to its basin stability, the latter to assess the accuracy of our bounds.

A. The Power Grid Model

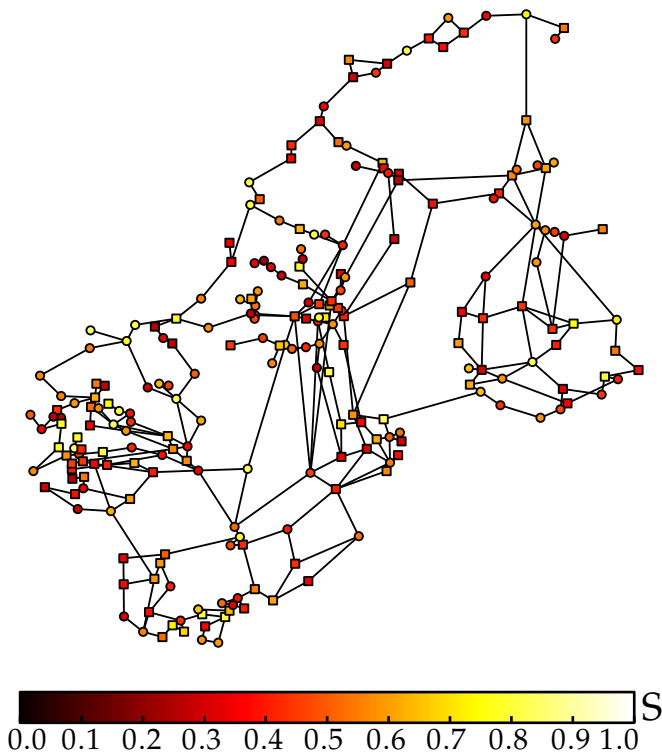


Figure 8. **Scandinavian power grid:** (Color online.) Network topology of the Scandinavian power grid. The nodes' colouring indicates the respective single-node survivability estimate. The frequency threshold is chosen as $\omega_{crit.} = \pm 5$ and initial conditions correspond to perturbations at a single node of the network sampled from the product set $[-\pi; \pi] \times [-5; 5]$. We randomly selected a dispatch scenario, circular nodes are net generators, squares are net consumers.

The dynamical system is given as

$$\begin{aligned} \dot{\phi}_i &= \omega_i \\ \dot{\omega}_i &= P_i - \alpha_i \omega_i - \sum_{j=1}^N K_{ij} \sin(\phi_i - \phi_j) \end{aligned} \quad (15)$$

with P_i being the net input power/consumption, α_i the electromechanical damping at node i and K_{ij} as the capacity of the link $i - j$. Here we choose $P_i = 1$ for net generators, $P_i = -1$ for net consumers, and a uniform distribution of $\alpha_i = \alpha = 0.1$.

The grid topology is that of the Scandinavian power grid [19], where we chose the nonzero K_{ij} equal to 6, corresponding to an average transmission line length of 200 km. The network consists of $N = 236$ nodes and 320 links, corresponding to a mean degree of $\bar{k} = 2.7$. Hence, the Scandinavian power grid has a sparse network topology with only a few neighbours per node on average, which is typical for power grids in general, independent from the number of nodes [32].

A stable operating state of the power grid is a fixed point of the dynamics with no frequency deviation, $(\phi^*, 0) := (\phi_1^*, \dots, \phi_N^*, 0, \dots, 0)$. The space we use to study the resilience of a single node n , given the current operating state of the system, is the space of states given by:

$$C_n = \{(\phi_1^*, \dots, \phi_n, \dots, \phi_N^*, 0, \dots, \omega_n, \dots, 0) \mid \phi_n \in [0, 2\pi), \omega_n \in \mathbb{R}\} \quad (16)$$

The desirable region being defined as $\forall i : |\omega_i| < 5$, which, as explained above, is chosen to mirror realistic constraints. Concretely, this means that we construct initial conditions by setting ϕ_i and ω_i to the value of the fixed point ϕ_i^* and 0, for all nodes other than the node n we are studying, and to a random phase in $[-\pi; \pi]$ as well as a random frequency deviation in $[-5; 5]$ for the node n . Then we simulate the system up to $t = 100$ and observe if, and if, when, any of the frequency deviations ω_i exceeds the threshold of the desirable region. In this way we sample 300 trajectories to estimate $S^n(t) := S^{C_n}(t)$.

In Fig. 8 we show the geographically embedded Scandinavian grid topology. The color of each node corresponds to the single-node conditional survivability $S^n(t = 100)$. As could be expected, different nodes exhibit vastly different resilience to perturbations. We postpone a detailed study of the impact of the network topology on survivability for future work. Instead we now turn to the question whether the semi-analytic bounds on the dynamics linearized around the fixed point, can accurately mirror the single-node survivability $S^n(t = 100)$.

Defining $\phi := (\phi_1, \dots, \phi_N)^T$, $\omega = (\omega_1, \dots, \omega_N)^T$ and $\alpha := \text{diag}(\alpha_i)$, the linearized dynamics is given by the Jacobian

$$\begin{pmatrix} \dot{\phi} \\ \dot{\omega} \end{pmatrix} = \begin{pmatrix} 0 & \mathbb{I}_N \\ L & -\alpha \end{pmatrix} \begin{pmatrix} \phi \\ \omega \end{pmatrix} \quad (17)$$

where the lower left block $(\partial \dot{\phi}_i / \partial \phi_j)$ can be identified with the Laplacian matrix (linearized around the fixed

point $(\phi^*, 0)$ given by

$$L_{ij} = \delta_{ij} \sum_{m=1}^N K_{im} \cos(\phi_i^* - \phi_m^*) - K_{ij} \cos(\phi_i^* - \phi_j^*) \quad (18)$$

The Jacobian has two real eigenvalues, namely $\lambda_1 = 0$ and $\lambda_2 = -\alpha$ corresponding to the eigenvectors $(\phi, \omega)_1 = (1, \dots, 0, \dots)$ and $(\phi, \omega)_2 = (-1/\alpha, \dots, 1, \dots)$. The first is the linearized version of the rotational symmetry of the system under shifting all elements of ϕ by the same amount ϕ_s : $\phi_i \mapsto \phi_i + \phi_s$. The second corresponds to a homogeneous shift of all oscillator's frequencies, which does not affect the phase differences, and decays exponentially due to the damping term. The remaining part of the spectrum consists of $N - 1$ pairs of complex conjugated eigenvalues.

B. Results

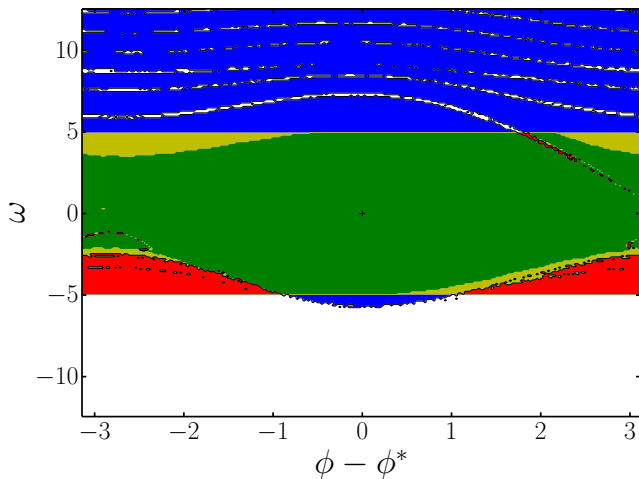


Figure 9. **single-node phase space classification:** (Color online.) The central green area resembles the infinite-time basin of survival, while the yellow and red areas contain finite-time surviving states. The union of the blue, yellow and green regions resembles the synchronous state's basin of attraction, while trajectories starting in the white or red regions approach different attractors. The frequency threshold is chosen as $\omega_{crit.} = \pm 5$ and initial conditions correspond to perturbations at a single consumer node of the network.

As in the two-node case, a large part of the single-node basin of attraction is centred around the fixed point $(\phi^*, 0)$, cf. Fig. 9. Within this region we expect the linear approximation to provide a lot of information on the system.

Regarding survivability, Fig. 10 shows that the frequency deviations inside the basin of attraction do indeed become large. The shape of the level lines of the frequency deviations corresponds to the basins of survival for different frequency constraints. The distorted

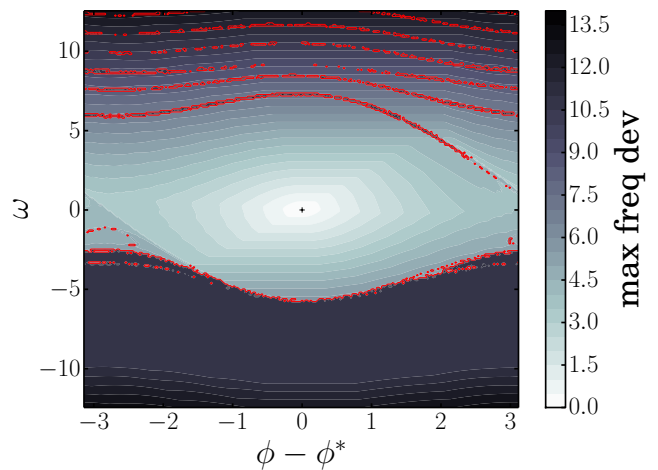


Figure 10. **Simulated maximum frequency deviations:** (Color online.) Field of the maximum frequency deviations along all dimensions, measured over the time evolution of the system for initial conditions that correspond to perturbations at a single node of the network. For comparison with Fig. 9, we give the basin of attraction's boundaries in red.

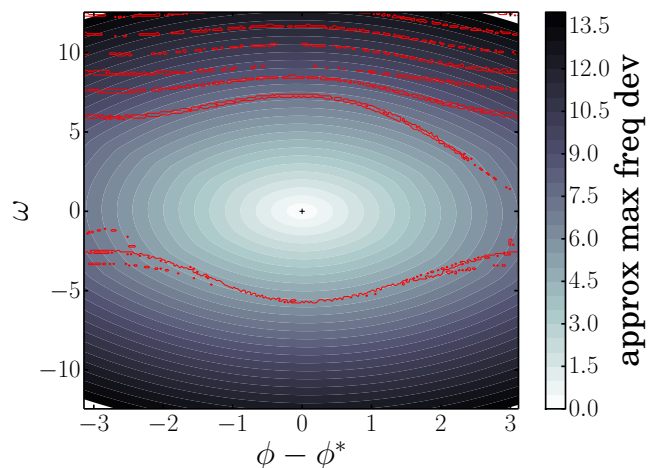


Figure 11. **Approximated maximum frequency deviations:** (Color online.) Analytic upper bound for the maximum frequency deviation (Eqn. 9) for the linear approximation. For comparison with Fig. 9, we give the basin of attraction's boundaries in red.

shape with the flat upper line is due to the fact that the basin of survival is bounded by in-spiraling trajectories starting at the edge of the desirable region.

Fig. 11 shows the bound for the frequency deviation of the linearized dynamics calculated according to Eqn. 9. This shows a good qualitative agreement with the actually simulated frequency deviations as long as the boundaries are relatively small. Still, the impact of the nonlinearity (e.g. multistability is not captured) on the system becomes apparent, especially further away from the fixed point.

Indeed Fig. 12 shows that there is a high correlation

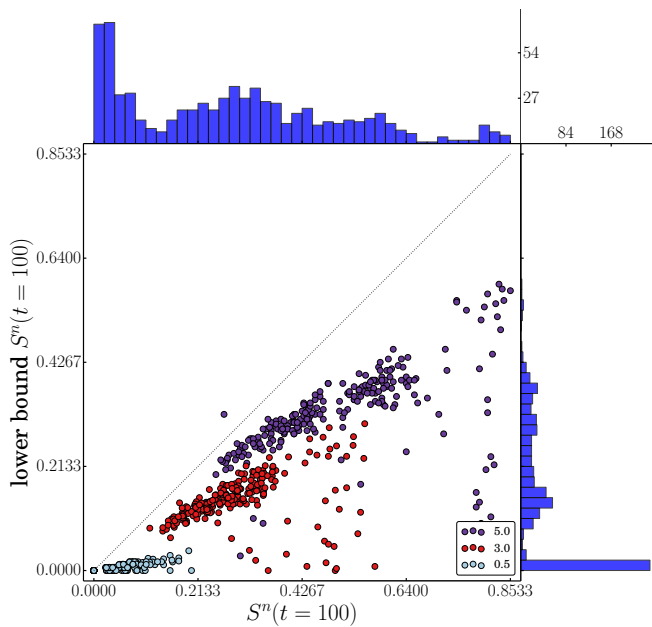


Figure 12. **Simulated vs. approximated single-node survivability:** (Color online.) Scatterplot of the simulated vs. approximated single-node survivability (cf. Eqn. 9) estimated for all nodes in the Scandinavian power grid ($\omega_{crit.}$ is indicated in the legend). The corresponding distributions are given besides.

between the lower bound of the survivability of the linear system calculated according to Eqn. 9 and the actual survivability at the majority of nodes for realistic values of frequency deviations. What exactly gives rise to the outliers far below the diagonal will require further study. Note that the computational cost of calculating the bounds on the maximum frequency deviation for a sample of initial conditions is many orders of magnitude lower than the numerical estimate of the survivability via simulations of the actual time evolution. For a realistic network size of several hundred nodes, the calculations can be performed on a laptop computer in less than a minute, whereas the survivability took about a day on 200 nodes of a computing cluster.

Finally Fig. 13 shows the single-node basin stability $SNBS$ as well as the single-node survivability of nodes in the Scandinavian power grid. We see that there is no significant correlation between the two quantities. This proves the point that the asymptotic behaviour of the system is not a strong indicator of the transient behaviour, at least in the case of power grids. The information we obtain from the survivability analysis is genuinely new information.

VI. CONCLUSIONS

Survivability is a resilience, respectively stability concept, that occupies a conceptually novel space between

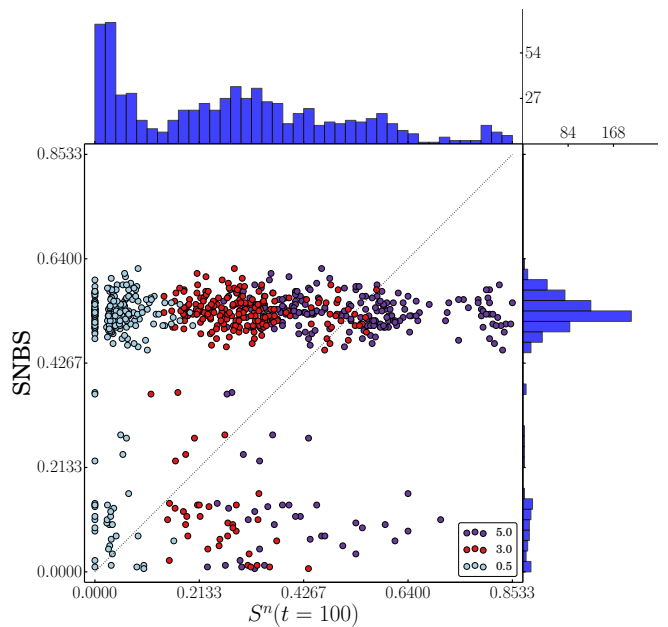


Figure 13. **Single-node basin stability vs. single-node survivability:** (Color online.) Scatterplot of the single-node basin stability vs. single-node survivability ($\omega_{crit.}$ is indicated in the legend) estimated for all nodes in the Scandinavian power grid. The corresponding distributions are given besides. Note that we have chosen the initial region X_0 for single-node basin stability with $|\omega| < 100$, the same region as in [19].

basin stability and other linear methods of asymptotic stability analysis.

It applies to linear and non-linear systems, in the absence and presence of multi-stability. It focuses on transient rather than asymptotic behaviour, and incorporates exogenous information via setting a desirable region for the system dynamics. Further, survivability can be estimated numerically at low computational costs, comparable to or even lower than for estimating basin stability.

For linear systems we provide easy to evaluate analytic and semi-analytic expressions for lower bounds of the survivability, with a trade-off between quality of the bound and numerical cost for evaluating the analytic expression. These eliminate the need to simulate the system, yielding further dramatic improvements in computational cost.

The bounds we find demonstrates that the survivability depends crucially on the eigenvectors of the linear dynamics, rather than the eigenvalues. It is an effective measure of the interaction between external constraints and the geometry of the dynamics in its phase space. The fact that the bound is tight, exactly when the analysis of asymptotic stability using the eigenvalues of the linearized system fails, shows that the survivability is genuinely complementary to eigenvalue-based stability concepts.

To explore this measure in practice we analyze three conceptual examples. Using a two-dimensional carbon

cycle model we see that survivability accurately shows the presence of dangerous transient behavior in the model, something that basin stability can not detect. Consequently it also allows us to see the trend towards the dangerous behavior becoming more common much earlier than basin stability, suggesting that it could improve on basin stability as a complementary early warning signal for tipping points. Just as for basin stability, the problem of evaluating the survivability from data remains a challenge for future work.

In the case of neuronal networks, the transients do not arise from a perturbation around a desirable state. Rather, the main interest lies on the transients themselves. Survivability reveals the same qualitative dependence of the dynamical behaviour on the underlying network topology as the average length of the transient studied in [41]. Beyond that considering $S(t)$ at fixed t as a function of the underlying topological parameters enables us to look in more detail into the relationship between function and structure of pulse coupled oscillator networks. In contrast to the average length of the transients, the survivability also has a direct conceptual interpretation as the probability of the system remaining in the interesting transient regime. Thus it captures the appropriate notion of resilience of the transient chaos against the global attractor.

The third conceptual example is a two-node power grid system. There we can see in detail the interplay between the semi-analytic bounds, that we developed, and the fully non-linear system.

This sets the stage for actually applying the survivability concept to the case of a realistic power grid. We demonstrate that survivability under realistic constraints captures information about the system not contained in the basin stability estimate. We also demonstrate that the semi-analytic lower bounds, are strongly correlated with the simulations of the non-linear dynamics. Thus they contain much of the relevant information about the system. In strategic power grid development studies, this fact becomes particularly important as computational power is often at a premium, due to the need to simulate a wide range of divergent future scenarios of the energy transition. Dynamical properties outside of quasi-stationary calculations, can only be taken into account if efficient estimators exist, it is not feasible to run simulations. Thus our lower bounds, which eliminate the need for such simulations, potentially enable a more systematic way to investigate the impacts of the energy transition. In particular, the influence of changing topologies and different distributions of dynamical parameters on the dynamics of the power grid become computationally accessible.

For the application to power grids, there are many more operational conditions on the system's behavior that we do not consider here. While not all of these are as amenable to analytic considerations as the frequency deviation, we anticipate that it will still be possible to find cheap analytic boundaries for them. The reason that

we could calculate the lower bounds so easily is that the phase space geometry is encoded in an efficient way in the eigenvectors. This aspect will carry over to many other, more complicated exogenous boundaries.

The work presented here thus opens up a plethora of new avenues of research. On the theoretical side, the existence of a closed form lower bound on the survivability of a linear system opens the door to study the survivability as a function of the network topology and system parameters analytically, especially for the optimisation of these parameters to increase the system's resilience. The lower bounds presented here can certainly be improved by taking the more detailed geometry of the trajectories of the linear system into account. It will also be important to extend them to the types of bounds we have in more realistic power grid models.

ACKNOWLEDGMENTS

We acknowledge gratefully the support of BMBF, CoNDyNet, FK. 03SF0472A, and Nora Molkenhain for illustrating our illustration of the concept of survivability using penguins.

Appendix A: Pulse-Coupled Integrate-and-Fire Oscillators

Firstly, the free dynamics of an oscillator j is given by

$$\dot{\phi}_j(t) = 1. \quad (\text{A1})$$

When an oscillator j reaches the threshold, $\phi_j(t) = 1$, its phase is reset to zero, $\phi_j(t^+) = 0$, and the oscillator emits a pulse that is sent to all oscillators i possessing an in-link from j . After a delay time τ this pulse induces a phase jump in the receiving oscillator i according to

$$\phi_i((t+\tau)^+) := \min \left(1, \frac{e^{b\varepsilon_{ij}} - 1}{e^b - 1} + e^{b\varepsilon_{ij}} \phi_i(t + \tau) \right) \quad (\text{A2})$$

The phase dependence is determined by a twice continuously differentiable function $U(\phi)$ that is assumed to be strictly increasing, $U'(\phi) > 0$, concave (down), $U''(\phi) < 0$, and normalized such that $U(0) = 0$ and $U(1) = 1$.

This model, originally introduced by Mirollo and Strogatz [22], is equivalent to different well known models of interacting threshold elements if $U(\phi)$ is chosen appropriately. Here we take functions of the form

$$U_b(\phi) = b^{-1} \ln(1 + (e^b - 1)\phi), \quad (\text{A3})$$

where $b > 0$ parameterizes the curvature of U , that determines the strength of the dissipation of individual oscillators. The function U approaches the linear, non-leaky case in the limit $\lim_{b \rightarrow 0} U_b(\phi) = \phi$. Other nonlinear

choices of $U \neq U_b$ give results similar to those reported above.

The considered graphs are strongly connected, i.e. there exists a directed path between any pair of nodes. We normalize the total input to each node $\sum_{j=1}^N \varepsilon_{ij} = \varepsilon$ such that the fully synchronous state exists. Furthermore for any node i all its k_i incoming links have the same strength $\varepsilon_{ij} = \varepsilon/k_i$.

Appendix B: Derivation of Analytic Bounds

As noted in the main text, the survivability of a linear system is amenable to analytic study. In this appendix we will give a detailed derivation of the results used in the main body of the text as well as some closely related ones.

1. Definitions:

We consider the case of a linear dynamic in $X = \mathbb{R}^N$, the standard Lebesgue measure $\text{Vol}(X) = \int_X dx^N$ and a polyhedral sunny region given by m linear conditions $y_k \cdot x(t) < 1$ for a set of vectors y_k , $k = 1 \dots m$ in \mathbb{R}^N .

The dynamics is given by a linear system of ordinary differential equations

$$\dot{x}(t) = Lx(t) \quad (\text{B1})$$

with $x \in X = \mathbb{R}^N$ and $L \in \mathbb{R}^{N \times N}$. In general, L has a complex spectrum, and we assume that all eigenvalues have non-positive real part. We denote the number of real eigenvalues of L as n_r , the number of pairs of complex conjugate complex eigenvalues n_c . Then we have a total of $n = n_r + n_c$ independent eigenvalues and $n_r + 2n_c = N$. We denote the eigenvalues as λ_i and $\bar{\lambda}_i$, and the corresponding eigenvectors as v_i and \bar{v}_i respectively.

Assuming that the real and imaginary parts of the eigenvectors of L span the entire space X , the general solution to the dynamical equations are then given by the matrix exponential

$$\begin{aligned} x(t) &= e^{Lt} x(0) \\ &= \sum_{j=1}^n \text{Re}(c_j e^{\lambda_j t} v_j) \\ &= \sum_{j=1}^{n_r} c_j e^{\lambda_j t} v_j + \sum_{j=n_r+1}^n \text{Re}(c_j e^{\lambda_j t} v_j), \end{aligned} \quad (\text{B2})$$

where the coefficients c_j are real for $j \leq n_r$ and complex above. To determine them we introduce a convenience map ι as follows:

$$\begin{aligned} \iota : \mathbb{R}^{n_r} \otimes \mathbb{C}^{n_c} &\rightarrow \mathbb{R}^N \\ \iota(c)_j &= \begin{cases} c_j & \text{if } j \leq n_r \\ \text{Re}(c_j) & \text{if } n_r < j \leq n_c \\ -\text{Im}(c_{(j-n_c)}) & \text{if } n_c < j. \end{cases} \end{aligned} \quad (\text{B3})$$

This is a real-linear map. Then we can define the real matrix \mathbb{V} as:

$$\begin{aligned} \mathbb{V} &= [v_1, \dots, v_{n_r}, \\ &\quad \text{Re}(v_{n_r+1}), \dots, \text{Re}(v_n), \\ &\quad -\text{Im}(v_{n_r+1}), \dots, -\text{Im}(v_n)]. \end{aligned} \quad (\text{B4})$$

and obtain

$$x(0) = (\mathbb{V} \circ \iota)(c), \quad (\text{B5})$$

which can be readily inverted as we assumed \mathbb{V} to have full rank.

2. Upper bound on the deviation of a single trajectory.

The inner product of $x(t)$ with a boundary vector $y \in \mathbb{R}^N$ is then simply given by:

$$y \cdot x(t) = \sum_{j=1}^{n_r} c_j e^{\lambda_j t} y \cdot v_j + \sum_{j=n_r+1}^{n_r+n_c} \text{Re}(c_j e^{\lambda_j t} y \cdot v_j) \quad (\text{B6})$$

Now, to obtain an upper bound on this for all times we can maximize each individual contribution. As the eigenvalues have non-positive real part each complex contribution has magnitude of at most $|c_j y \cdot v_j|$. The maximum of the real contribution depends on the sign of $c_j y \cdot v_j$ and is given by

$$\max(0, c_j y \cdot v_j) \quad (\text{B7})$$

unless $\lambda_j = 0$ in which case the contribution is exactly equal $c_j y \cdot v_j$. While this does not happen generically it occurs due to symmetries in the system, and thus we will treat it separately. We denote the number of zero eigenvalues by n_0 . We have:

$$\begin{aligned} \max_{t \in [0; \infty[} |y \cdot x(t)| &\leq \sum_{j=1}^{n_0} c_j y \cdot v_j \\ &+ \sum_{j=n_0+1}^{n_r} \max(0, c_j y \cdot v_j) \\ &+ \sum_{j=n_r+1}^n |c_j y \cdot v_j|. \end{aligned} \quad (\text{B8})$$

This is the key approximation for our analysis. In the next section we will use this estimate to give a lower bound for the total survivability, afterwards we will show when this bound becomes tight.

3. A lower bound for the total survivability

For a boundary vector y_k let us define $y_{kj} = y_k \cdot v_j$ for $j \leq n_r$ and $y_{kj} = |y_k \cdot v_j|$ for $n_r < j \leq n$. Then the inequalities

$$\sum_{j=1}^{n_0} y_{kj} c_j + \sum_{j=n_0+1}^{n_r} \max(0, y_{kj} c_j) + \sum_{j=n_r+1}^n y_{kj} |c_j| < 1 \quad (\text{B9})$$

define a region V_c in $\mathbb{R}^{n_r} \otimes \mathbb{C}^{n_c}$ that is mapped to a subset of X_∞^S by the linear transformation $\mathbb{V} \circ \iota$. This is a subset of X_∞^S as the initial conditions in this region have an inner product with the boundary vectors y_k bounded by Eqn. B8. Thus, taking the effect of the transformation \mathbb{V} into account, we have the lower bound

$$\text{Vol}(X_\infty^S) \geq \sqrt{\det \mathbb{V} \mathbb{V}^T} \text{Vol}(V_c). \quad (\text{B10})$$

$$\mathbb{T} = \left\{ \sum_{j=1}^{n_r} c_j v_j + \text{Re} \left(\sum_{j=n_r+1}^n c_j e^{i\phi_j} v_j \right) \middle| \phi_j \in [0; 2\pi[\right\} \quad (\text{B11})$$

The maximum of the torus along the y direction is obtained exactly by maximizing each contribution independently, which means tuning the ϕ_i so that $c_j e^{i\phi_j} \hat{x} \cdot v_j$ are real, thus the real part equals the absolute value:

$$\max_{\phi_i \in [0; 2\pi[} |y \cdot \mathbb{T}| \leq \sum_{j=1}^{n_r} c_j y \cdot v_j + \sum_{j=n_r+1}^n |c_j y \cdot v_j| \quad (\text{B12})$$

with equality if $\frac{\text{Im}(\lambda_i)}{\text{Im}(\lambda_j)}$ is irrational. Therefore, in this case, the general bound Eqn. B8 holds with equality. We have:

$$\max_{t \in [0; \infty[} |y \cdot x(t)| = \sum_{j=1}^{n_r} c_j(x_0) y \cdot v_j + \sum_{j=n_r+1}^n |c_j(x_0)| |y \cdot v_j| \quad (\text{B13})$$

and therefore also

$$\text{Vol}(X_\infty^S) = \sqrt{\det \mathbb{V} \mathbb{V}^T} \text{Vol}(V_c). \quad (\text{B14})$$

This bound can be evaluated numerically quite easy. All that is needed is to sample X^+ and take the fraction of samples for which the image under the linear map $(\mathbb{V} \circ \iota)^{-1}$ satisfies Eqn. B9. This also makes it very easy to numerically estimate the lower bound of conditional survivability, by sampling from $C \cap X^+$ instead. In that way, Fig. 7 and Fig. 11 were created.

In order to proceed with the analytic calculations we have to consider further special cases. First we will show that the bound Eqn. B10 is actually exact for some cases.

4. The case of vanishing real parts.

Let us now consider the case where the real part of all λ_i is zero, and $\frac{\text{Im}(\lambda_i)}{\text{Im}(\lambda_j)}$ is irrational. Thus $n_0 = n_r$. In that case the trajectory with initial conditions $x(0) = \mathbb{V} \circ \iota \circ c$ is dense on the torus:

5. The purely imaginary case.

For the case $n_r = n_0 = 0$ we can give an explicit lower bound for $\text{Vol}(V_c)$. To do so, define $\tilde{y}_j = \min_k y_{k'j}$. The volume of the space \tilde{V}_c defined by the inequality

$$\sum_{j=1}^n \tilde{y}_j |c_j| < 1 \quad (\text{B15})$$

is a lower bound for the volume of V_c . The two spaces have the same volume if there is one condition that dominates all others, that is, if there is a k' such that $\tilde{y}_j = y_{k'j}$ for all j . This means that any trajectory that leaves the allowed region also crosses the boundary defined by $x \cdot y_k \leq 1$.

We now need to evaluate the $2n = 2n_c = N$ dimensional integral

$$\text{Vol}(\tilde{V}_c) = \int_{\tilde{V}_c} \prod_{j=1}^n dc_j^r dc_j^i, \quad (\text{B16})$$

with $c_j = c^r + ic_j^i$. We begin by changing $dc_j^r dc_j^i$ to polar coordinates $r_j dr_j d\phi_j$ and rescaling:

$$\begin{aligned} \text{Vol}(\tilde{V}_c) &= \left(\prod_j \tilde{y}_j^2 \right) \int_{\sum_j r_j < 1} \prod_{j=1}^n r_j dr_j d\phi_j \\ &= (2\pi)^n \int_{\sum_j r_j < 1} \prod_{j=1}^n r_j dr_j. \end{aligned} \quad (\text{B17})$$

The integral can now be written as

$$\text{Vol}(\tilde{V}_c) = \left(\prod_j \tilde{y}_j^2 \right) (2\pi)^n \int_0^{1-\sum_{j>1} r_j} r_1 dr_1 \int_0^{1-\sum_{j>2} r_j} r_2 dr_2 \int_0^{1-\sum_{j>3} r_j} r_3 dr_3 \dots \quad (\text{B18})$$

This can be calculated by beta functions[26]:

$$\text{Vol}(\tilde{V}_c) = \frac{(2\pi)^n}{(2n+1)!} \prod_j \tilde{y}_j^2. \quad (\text{B19})$$

This finally means that we obtain the lower bound on the region of total survivability of a linear system with

no real eigenvalues and all real parts of the eigenvalues equal to zero of

$$\text{Vol}(X_\infty^S) \geq \frac{(2\pi)^n}{(2n+1)!} \sqrt{\det \mathbb{V}\mathbb{V}^T} \prod_j \tilde{y}_j^2. \quad (\text{B20})$$

-
- [1] J. Alexander, J. Yorke, Z. You, and I. Kan. Riddled basins. *International Journal of Bifurcation and Chaos*, 2(4):795–813, 1992.
- [2] J. M. Anderies, S. R. Carpenter, W. Steffen, and J. Rockström. The topology of non-linear global carbon dynamics: from tipping points to planetary boundaries. *Environmental Research Letters*, 8:044048, 2013.
- [3] V. Anishchenko, V. Astakhov, A. Neiman, T. Vadivasova, and L. Schimansky-Geier. *Dynamics of Chaotic and Stochastic Systems*. Springer, Berlin, 2006.
- [4] J.-P. Aubin. Viability Kernels and Capture Basins of Sets Under Differential Inclusions. *SIAM Journal on Control and Optimization*, 40(3):853–881, 2001.
- [5] J.-P. Aubin, A. Bayen, and P. Saint-Pierre. *Viability Theory. New Directions*. Springer Science & Business Media, 2011.
- [6] V. N. Belykh, I. V. Belykh, and M. Hasler. Connection graph stability method for synchronized coupled chaotic systems. *Physica D: Nonlinear Phenomena*, 195(1-2):159–187, 2004.
- [7] N. Bonneuil. Computing the viability kernel in large state dimension. *Journal of Mathematical Analysis and Applications*, 323:1444–1454, 2006.
- [8] H.-D. Chiang. *Direct Methods for Stability Analysis of Electric Power Systems*. John Wiley & Sons, Inc., Hoboken, NJ, USA, 2010.
- [9] F. Dörfler, M. Chertkov, and F. Bullo. Synchronization in complex oscillator networks and smart grids. *Proceedings of the National Academy of Sciences of the United States of America*, 110(6):2005–10, 2013.
- [10] W. Ebeling and I. M. Sokolov. *Statistical Thermodynamics and Stochastic Theory of Nonequilibrium Systems*. World Scientific, Singapore, 2005.
- [11] U. Ernst, K. Pawelzik, and T. Geisel. Synchronization induced by temporal delays in pulse-coupled oscillators. *Physical Review Letters*, 74:1570, 1995.
- [12] U. Feudel and C. Grebogi. Why are chaotic attractors rare in multistable systems? *Physical Review Letters*, 91(13):134102, 2003.
- [13] G. Filatrella, A. H. Nielsen, and N. F. Pedersen. Analysis of a power grid using a Kuramoto-like model. *The European Physical Journal B*, 61(4):485–491, 2008.
- [14] J. Heitzig and T. Kittel. Topology of sustainable management of dynamical systems with desirable states. *Earth System Dynamics*, in review.
- [15] S. Jahnke, R.-M. Memmesheimer, and M. Timme. Stable irregular dynamics in complex neural networks. *Physical Review Letters*, 100(4):048102, 2008.
- [16] P. Ji, T. K. D. Peron, P. J. Menck, F. A. Rodrigues, and J. Kurths. Cluster Explosive Synchronization in Complex Networks. *Physical Review Letters*, 110(21):218701, 2013.
- [17] Y. Lai and C. Grebogi. Intermingled basins and two-state on-off intermittency. *Physical Review E*, 1995.
- [18] J. N. Maidens, S. Kaynama, I. M. Mitchell, M. M. K. Oishi, and G. a. Dumont. Lagrangian methods for approximating the viability kernel in high-dimensional systems. *Automatica*, 49:2017–2029, 2013.
- [19] P. J. Menck, J. Heitzig, J. Kurths, and H. J. Schellnhuber. How dead ends undermine power grid stability. *Nature Communications*, 5:1–8, 2014.
- [20] P. J. Menck, J. Heitzig, N. Marwan, and J. Kurths. How basin stability complements the linear-stability paradigm. *Nature Physics*, 9(2):89–92, 2013.
- [21] J. Milnor. On the concept of attractor. *Communications*

- in *Mathematical Physics*, 99(2):177–195, 1985.
- [22] R. Mirollo and S. Strogatz. Synchronization of pulse-coupled biological oscillators. *Siam Journal on Applied Mathematics*, 50(6):366, 1990.
- [23] A. E. Motter, S. A. Myers, M. Anghel, and T. Nishikawa. Spontaneous synchrony in power-grid networks. *Nature Physics*, 9(3):191–197, 2013.
- [24] T. Nishikawa and A. E. Motter. Synchronization is optimal in nondiagonalizable networks. *Physical Review E*, 73(6):065106, 2006.
- [25] T. Nishikawa and A. E. Motter. Comparative analysis of existing models for power-grid synchronization. *New Journal of Physics*, 17(1):15012, 2015.
- [26] The detailed calculation can be found here <http://math.stackexchange.com/a/207605>. (Accessed: June 3, 2015).
- [27] H. E. Nusse and J. A. Yorke. Basins of attraction. *Science*, 271:1376–1380, 1996.
- [28] H. E. Nusse and J. A. Yorke. Wada basin boundaries and basin cells. *Physica D: Nonlinear Phenomena*, 90:242–261, 1996.
- [29] L. M. Pecora and T. L. Carroll. Master Stability Functions for Synchronized Coupled Systems. *Physical Review Letters*, 80(1):2109–2112, 1998.
- [30] A. N. Pisarchik and U. Feudel. Control of multistability. *Physics Reports*, 540(4):167–218, 2014.
- [31] J. Rockström, W. Steffen, K. Noone, A. Persson, F. S. Chapin, E. F. Lambin, T. M. Lenton, M. Scheffer, C. Folke, H. J. Schellnhuber, B. Nykvist, C. A. de Wit, T. Hughes, S. van der Leeuw, H. Rodhe, S. Sörlin, P. K. Snyder, R. Costanza, U. Svedin, M. Falkenmark, L. Karlberg, R. W. Corell, V. J. Fabry, J. Hansen, B. Walker, D. Liverman, K. Richardson, P. Crutzen, J. A. Foley, and E. Al. A safe operating space for humanity. *Nature*, 461(September):472–475, 2009.
- [32] P. Schultz, J. Heitzig, and J. Kurths. A random growth model for power grids and other spatially embedded infrastructure networks. *The European Physical Journal Special Topics*, 223(12):1–18, 2014.
- [33] P. Schultz, J. Heitzig, and J. Kurths. Detours around Basin Stability in Power Networks. *New Journal of Physics*, 16(12):125001, 2014.
- [34] M. D. Shrimali, A. Prasad, R. Ramaswamy, and U. Feudel. The Nature of Attractor Basins in Multistable Systems. *International Journal of Bifurcation and Chaos*, 18(06):1675–1688, 2008.
- [35] T. Tél. Transient Chaos. In B.-l. Hao, editor, *Directions in Chaos*, volume 3, pages 149–221. World Scientific, Singapore, 1990.
- [36] T. Tél. Transient chaos: a type of metastable state. In *STATPHYS 19 (the 19th IUPAP Int. Conf. on Stat. Phys. Xiamen, China, 31 July-4 Aug. 1995)*, pages 346–362. 1996.
- [37] UCTE. Continental Europe Operation Handbook, Glossary. Technical report, 2004.
- [38] T. Weckesser, H. Johannsson, and J. Ostergaard. Impact of model detail of synchronous machines on real-time transient stability assessment. In *2013 IREP Symposium Bulk Power System Dynamics and Control - IX Optimization, Security and Control of the Emerging Power Grid*, pages 1–9. IEEE, 2013.
- [39] A. T. Winfree. *The geometry of biological time*. Springer, New York, 2001.
- [40] M. Wolfrum and O. E. Omel’chenko. Chimera states are chaotic transients. *Physical Review E - Statistical, Nonlinear, and Soft Matter Physics*, 84(1):2–5, 2011.
- [41] A. Zumdieck, M. Timme, T. Geisel, and F. Wolf. Long Chaotic Transients in Complex Networks. *Physical Review Letters*, 93(24):244103–4, 2004.
- [42] D. Zwillinger. *Handbook of differential equations*. Academic Press, 3rd edition, 1997.